Interplay of the Kondo effect with the induced pairing in electronic and caloric properties of T-shaped double quantum dots

Krzysztof P. Wójcik[1,2,*] and Ireneusz Weymann[2]

[1]*Institute of Molecular Physics, Polish Academy of Sciences, Smoluchowskiego 17, 60-179 Poznań, Poland*

[2]*Faculty of Physics, Adam Mickiewicz University, Umultowska 85, 61-614 Poznań, Poland*

(Received 23 April 2018; published 27 June 2018)

We examine the influence of the superconducting proximity effect on the transport properties of a T-shaped double quantum dot strongly coupled to two normal, nonmagnetic or ferromagnetic leads. We show that the two-stage Kondo screening may be suppressed or enhanced by the presence of pairing correlations, depending on the specific geometric arrangement of the device. We explain our results by invoking an effective decrease of Coulomb interactions by the proximity effect and find a qualitatively correct description in many cases, although the spin-filtering effect stemming from spin-dependent Fano-Kondo interference is surprisingly vulnerable to the presence of induced superconducting pairing correlations. The results are obtained within the numerical renormalization group framework in the limit of large superconducting gap, which allows for a reliable examination of the low-temperature subgap properties of the considered system. Nevertheless, finite-temperature effects are also taken into account.

DOI: 10.1103/PhysRevB.97.235449

I. INTRODUCTION

The two-stage Kondo effect in double quantum dots (DQDs) or double magnetic impurities has been studied for over a decade, both theoretically [1–10] and experimentally [11,12], in various contexts. In particular, its relation to the Fano-like interference [13–15] was precisely established [6] and the spin-dependent variant of this effect for DQDs in an external magnetic field [16] or coupled to ferromagnetic leads [17] was proposed as a method for obtaining electrically tunable spin-polarized currents. Moreover, the Andreev transport properties of T-shaped DQDs coupled to superconducting (SC) and normal leads have also been considered [18–23]. In such hybrid systems, for low temperatures and voltages smaller than the superconducting energy gap, transport occurs due to Andreev reflection processes [24–26]. However, while most studies dealt with transport between normal and superconducting electrodes, the normal electronic and caloric transport through T-shaped DQDs coupled to two normal (ferromagnetic) leads and proximized by the third, superconducting electrode, has hardly been examined so far. Therefore, in this paper, we perform a detailed and accurate analysis of such a case.

To begin with, it is instructive to notice that similar studies of a single quantum-dot case unveiled an intriguing interplay between the Kondo physics [27,28] and the pairing induced by the superconducting contact [29–32]. A hallmark of this interplay is a quantum phase transition between the Kondo-screened singlet and the BCS-like singlet states, as the ratio of the Kondo temperature to the superconducting energy gap is varied [31,32]. At the Kondo side of the transition, the Kondo temperature was found to be enhanced with increasing the coupling strength to the superconducting lead [33,34]. At the other side, Yu-Shiba-Rusinov-like bound states [35–37] are formed, which have already been explored experimentally with the Andreev bias spectroscopy [38]. The quantum phase transition is present only in the absence of the normal leads and gets smeared to a crossover otherwise. Nevertheless, even in the latter case, around the critical value of the quantum-dot–SC coupling, the BCS-like expectation value $\langle d_\uparrow d_\downarrow \rangle$ for spin-σ quantum dot annihilation operators d_σ becomes nonzero [34].

In this paper, we show that the interplay of the superconducting proximity effect and correlations giving rise to the Kondo effect is even more interesting if a single quantum dot is substituted by a T-shaped DQD; see Fig. 1. In this geometry, one quantum dot (QD1 in Fig. 1) is embedded between two normal (ferromagnetic) leads and coupled to the second quantum dot (QD2). We consider two possible scenarios, in which the superconductor is coupled to either the first or the second quantum dot. Then, depending on which quantum dot is proximized and what is the strength of the coupling to SC lead, different interesting effects take place, as described in the following. They include, among others, an enhancement and a destruction of any of the two screening stages of the Kondo phenomenon.

Since one of the most experimentally accessible physical quantities of such a system is its conductance, we base our discussion on the dependence of conductance on model parameters, gate voltages, and temperature. This allows us to thoroughly examine the influence of induced superconducting pairing on the two stages of the Kondo effect. Moreover, further information is gained from the analysis of the Seebeck coefficient, the so-called thermopower, whose sign and magnitude change between different Kondo states [10,39–44], while temperature dependence allows for recognizing metallic and hoppinglike transport regimes [44,45].

We note that the subgap transport through hybrid double quantum-dot systems is currently undergoing an extensive

*kpwojcik@ifmpan.poznan.pl

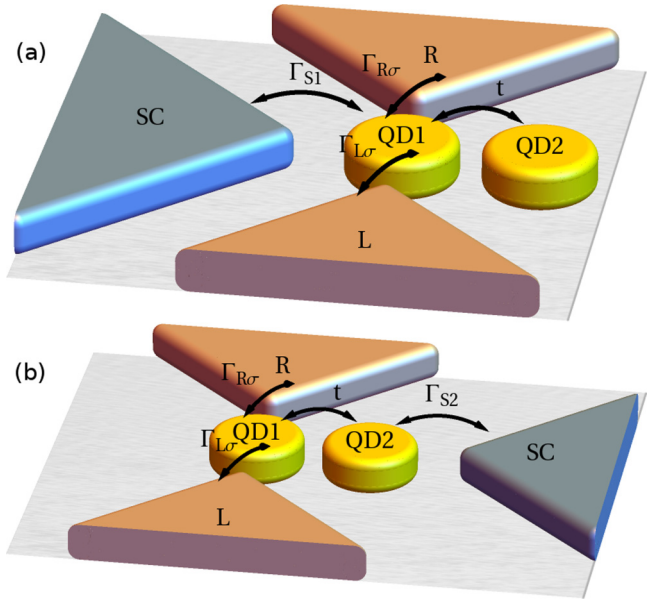

FIG. 1. Schemes of possible realizations of the considered system. The first quantum dot (QD1) is coupled to the left and right normal (ferromagnetic) leads with coupling strength $\Gamma_{r\sigma}$, where $r = L/R$ for the left/right lead. The two dots are coupled via hopping matrix elements t. The superconducting electrode can be attached either to (a) the first ($i = 1$) or (b) the second ($i = 2$) quantum dot, with the corresponding coupling strength Γ_{Si}.

exploration. This has been stimulated by impressive experiments demonstrating controllable splitting of Cooper pairs in DQDs with both dots attached to a superconductor [46]. This has also provided great motivation to many researchers to analyze hybrid DQDs in terms of their Cooper pair splitting efficiency. This is an undoubtedly interesting direction; however, here we focus on completely different geometry, with only one quantum dot directly coupled to the SC lead. While being less useful as a Cooper pair splitter, this system exhibits very interesting strongly correlated physics. Simultaneously, recent rapid experimental advances in the field [47–54] give hope for a possibility of fabricating the device considered here. From this point of view, our results are expected to stimulate further research in hybrid T-shaped DQDs as well as to be of assistance in understanding future experimental observations.

It is interesting to note that the interplay between the Kondo correlations and superconductivity has also been considered in the case of the Anderson model with attractive on-site Coulomb interactions [55]. In such a case, the charge Kondo effect may occur, manifesting itself in the electronic [56], caloritronic [57], and spin-caloritronic [58] properties. Moreover, intensive theoretical and experimental investigations have clearly shown that in Tl-doped PbTe, the negative-U centers induce superconductivity in the otherwise normal host, while the charge Kondo effect takes place in the system [59–63]. The charge Kondo effect is, however, not present in our system. Instead of attractive-U center influence on the normal host, we examine the influence of the BCS superconductor on a DQD structure. Furthermore, recent experiments have also demonstrated the possibility of fabricating quantum dots with attractive Coulomb interactions, which persist both below and above the critical temperature for the superconducting transition in the leads [64,65]. This gives rise to an interesting interplay between the electrostatic attraction and pairing, which leads to suppression of the supercurrent through the device in the crossover region between the weak-coupling and strong-coupling unitary transmission regimes [66]. Moreover, unlike the spin Kondo effect, its charge counterpart may become enhanced under nonequilibrium spin bias [67]. Although in this paper we focus on the repulsive-U case, our work shall contribute to the general understanding of the interplay between Kondo correlations with the superconducting proximity effect.

The paper has the following structure. In Sec. II, a detailed description of the model is provided. Section III briefly summarizes the role of the magnitude of Coulomb interactions for further reference. The results for the case of QD1 (QD2) coupled to the SC lead are then presented in Sec. IV (Sec. V), respectively, and the paper is summarized in Sec. VI.

II. MODEL

In the present paper, we consider the T-shaped double quantum dot (DQD) coupled to two metallic (in general ferromagnetic) leads, and proximized by one superconducting electrode. We analyze two possible realizations of such system, in which the SC lead is attached either to the first [Fig. 1(a)] or to the second [Fig. 1(b)] quantum dot. In both cases, the Hamiltonian of the system can be written in the general form $H = H_{\rm DQD} + H_{\rm L} + H_{\rm R} + H_{\rm T} + H_{\rm S} + H_{\rm TS}$, where the subsequent parts describe the isolated DQD, left and right leads, tunneling between DQD and these leads, superconductor, and, finally, the tunneling between SC and DQD, respectively.

We assume that the normal leads contain quasifree electrons, $H_r = \sum_{\mathbf{k}\sigma} \varepsilon_{r\mathbf{k}\sigma} c^\dagger_{r\mathbf{k}\sigma} c_{r\mathbf{k}\sigma}$, with $r \in \{R,L\}$ and $c_{r\mathbf{k}\sigma}$ denoting the annihilation operator corresponding to the electron in lead r possessing pseudomomentum $\mathbf{k}$ and spin σ. $H_{\rm T}$ has a form of spin-preserving local hopping between QD1 and the electrodes, $H_{\rm T} = \sum_{r\mathbf{k}\sigma} v_{r\mathbf{k}} d^\dagger_{1\sigma} c_{r\mathbf{k}\sigma}$, where $d_{i\sigma}$ annihilates the spin-σ electron at QDi. Assuming the wideband situation, for the hybridization function between QD1 and lead r we take a constant within the energy cutoff $\pm D$ around the Fermi level, $\Gamma_{r\sigma} = \pi\rho_{r\sigma}|v_{kr}|^2$, where $\rho_{r\sigma}$ is the (spin-resolved) normalized density of states in the lead r at the Fermi level. With these approximations, the ferromagnetism of normal leads can be taken into account through the spin dependence of $\Gamma_{r\sigma} = \Gamma_r(1 + p_r\sigma)$, where p_r is the spin polarization in the lead r, provided their magnetization is parallel. We also assume symmetric couplings, $\Gamma_r = \Gamma/2$, and $p_{\rm L} = p_{\rm R} = p$.

In the present paper, we focus on the low-temperature physics. Therefore, having written $H_{\rm S}$ in the BCS form, $H_{\rm S} = \sum_{\mathbf{k}\sigma} \varepsilon_{\mathbf{k}} c^\dagger_{\mathbf{k}\sigma} c_{\mathbf{k}\sigma} + \sum_{\mathbf{k}} (\Delta_{\mathbf{k}} c^\dagger_{\mathbf{k}\uparrow} c^\dagger_{\mathbf{-k}\downarrow} + {\rm H.c.})$, we assume isotropic pairing amplitude, $\Delta_{\mathbf{k}} = \Delta > 0$, and integrate out the single-electron states of the superconductor lying outside the energy gap $2|\Delta|$, to finally take the limit of $|\Delta| \to \infty$ [29,30]. In this way, we obtain an effective Hamiltonian $H_{\rm eff} = H_{\rm SDQD} + H_{\rm L} + H_{\rm R} + H_{\rm T}$, with SC-proximized DQD part

$$H_{\rm SDQD} = \sum_{i\sigma} \varepsilon_i n_{i\sigma} + \sum_i U_i n_{i\uparrow} n_{i\downarrow} + U'(n_1 - 1)(n_2 - 1) + t \sum_\sigma (d^\dagger_{1\sigma} d_{2\sigma} + {\rm H.c.}) - \Gamma_{Si}(d^\dagger_{i\uparrow} d^\dagger_{i\downarrow} + {\rm H.c.}), \quad (1)$$

where ε_i is the energy level of QDi, U_i denotes the respective Coulomb interaction strength, U' measures interdot Coulomb interactions, t is the interdot hopping matrix element, and Γ_{Si} describes the coupling to the superconductor of QDi ($i = 1$ or 2, depending on geometry). The operator $n_i = n_{i\uparrow} + n_{i\downarrow}$, while $n_{i\sigma} = d^\dagger_{i\sigma} d_{i\sigma}$. Henceforth, we use the detuning $\delta_i = \varepsilon_i + U_i/2$ from the particle-hole symmetry point of each dot to specify the energy levels of the QDs. The coupling Γ_{Si} is related to the hopping matrix element v_{Si} between QDi and SC, and the normalized density of states of SC in the normal state, ρ_S, through $\Gamma_{Si} = \pi\rho_S|v_{Si}|^2$, and it is assumed to be energy independent, similarly to the normal leads case. The negative sign in front of Γ_{Si} corresponds to the choice of real and positive Δ in the bulk superconductor Hamiltonian. The second quantum dot QD2 is, by assumption, coupled to the normal leads only indirectly, through QD1; compare Fig. 1. Through an even-odd change of basis of the leads states [68], the model at equilibrium can be exactly mapped onto an effective single-band system, possessing an effective coupling Γ and a spin polarization p.

Then, the model is solved with the aid of the numerical renormalization group (NRG) technique [69,70]. We use the complete basis set [71,72] to construct the full density matrix of the system [73]. Once the energy spectrum of the discretized Hamiltonian is known, the spin-resolved transmission coefficient $\mathcal{T}_\sigma(\omega) = -\Gamma_\sigma \mathrm{Im}\langle\langle d_{1\sigma}; d^\dagger_{1\sigma}\rangle\rangle^{\mathrm{ret}}(\omega)$ is calculated from the imaginary part of the Fourier transform of the retarded QD1 Green's function. The transport coefficients, such as the linear-response conductance in spin channel σ, G_σ, and the thermopower S, can be calculated from $\mathcal{T}_\sigma(\omega)$ using the standard linear-response expressions

$$G_\sigma = \frac{e^2}{h} L_{0\sigma}, \tag{2}$$

$$S = -\frac{1}{eT}\frac{L_{1\uparrow} + L_{1\downarrow}}{L_{0\uparrow} + L_{0\downarrow}}, \tag{3}$$

with $L_{n\sigma} = \sum_\sigma \int \omega^n [-\partial f_T(\omega)/\partial\omega]\mathcal{T}_\sigma(\omega) d\omega$, $f_T(\omega)$ denoting the Fermi-Dirac distribution function, e (minus) the electron charge, and h the Planck constant. The spin-dependent conductance allows for determining the linear-response current spin polarization through $\mathcal{P} = (G_\uparrow - G_\downarrow)/G$, with the total conductance $G = G_\uparrow + G_\downarrow$. In NRG calculations, at least 2048 states per iteration were kept and the discretization parameter $\Lambda = 2$ was used, while the quantities of interest were calculated directly from discrete data [74].

While neglecting the presence of the states of the superconductor lying outside the gap is one of the strongest limitations of the presented model, one needs to keep in mind that at low temperatures, these states contribute quite weakly to the physics of the real systems. Moreover, the device is coupled to another continuum, namely, to normal leads. Therefore, one can expect that the effects of the presence of the gapped continuous part of the spectrum of the SC lead are only quantitative and rather weak at low temperatures. Nevertheless, detailed study of a single quantum dot coupled to a superconductor [75] shows the sign change of the order parameter at the singlet-doublet transition point, which is necessarily not captured in our model for the quantum dot directly coupled to the SC electrode.

III. THE ROLE OF COULOMB INTERACTIONS

One of the most intuitive consequences of the presence of a pairing potential induced by SC proximity is an effective reduction of the corresponding Coulomb repulsion. To be able to analyze the range of validity of this picture, first we summarize the effects related to the on-dot and interdot capacitative correlations, U_i and U', for further reference. Therefore, in this section, we consider the system in the absence of SC lead.

A. Influence on Kondo screening

The essence of the Kondo effect is the screening of the local moment by the conduction-band electrons [27]. Since Coulomb interactions are inevitable for the formation of such a moment, they are clearly necessary for the Kondo physics to occur. However, it should also be noted that for $U \gtrsim 4\Gamma/\pi$, which is the most common situation, the Kondo temperature T_K is a decreasing function of U due to its exponential dependence on Γ/U [76].

In T-shaped DQDs, the Kondo effect develops in two stages [4]. When the temperature is lowered, first, the magnetic moment of QD1 is screened by the conduction electrons of the leads at the Kondo temperature T_K. Then, for $T \ll T_K$, the resulting Fermi liquid serves as a band of the halfwidth $\sim T_K$ for the second quantum dot (QD2), the magnetic moment of which is screened at the second stage of the Kondo effect, with the corresponding Kondo temperature [4]

$$T^* \sim T_K \exp(-T_K/J), \tag{4}$$

where J is an effective antiferromagnetic exchange interaction between the two dots, $J \sim t^2/U$. Note that estimations of T_K or T^*, such as Eq. (4), possess rather an order-of-magnitude precision and for qualitative comparison of Kondo temperatures in different systems, a more precise definition is necessary. Here, we follow the convention of defining T_K as a temperature at which the conductance increases to half of its maximal value as the temperature is lowered, such that $G(T_K) = G_{\max}/2$, with $G_{\max}$ being the global maximum of $G(T)$. Moreover, in this paper, by T_K we mean in fact the Kondo temperature in the case of $t = 0$. Furthermore, in a similar fashion, we can define T^* as the temperature below T_K at which $G(T)$ drops to $G_{\max}/2$ again (this happens only for $t \neq 0$).

The picture of the two-stage screening presented above does not include the influence of capacitive coupling between the two dots, U', which will be discussed now. Figure 2 demonstrates how finite values of U' influence the Kondo physics in the considered nanostructure, depending on detuning of QD1 δ_1 from the particle-hole symmetry (PHS) point, $\delta_1 = 0$, in the case of nonmagnetic ($p = 0$) and ferromagnetic ($p = 0.5$) metallic leads. In Fig. 2(a), one can see that the second-stage Kondo temperature T^* is indeed increased by finite U'. In fact, the effective exchange coupling J increases by a factor $(1 - U'/U)^{-1}$ for finite capacitive coupling between the dots [7]. However, qualitative features remain the same. At PHS, with lowering the temperature, the conductance first increases at T_K and almost reaches $2e^2/h$. Then, it decreases to 0 for temperatures below T^*. This behavior is observed for both ferromagnetic and nonmagnetic leads, although only at the

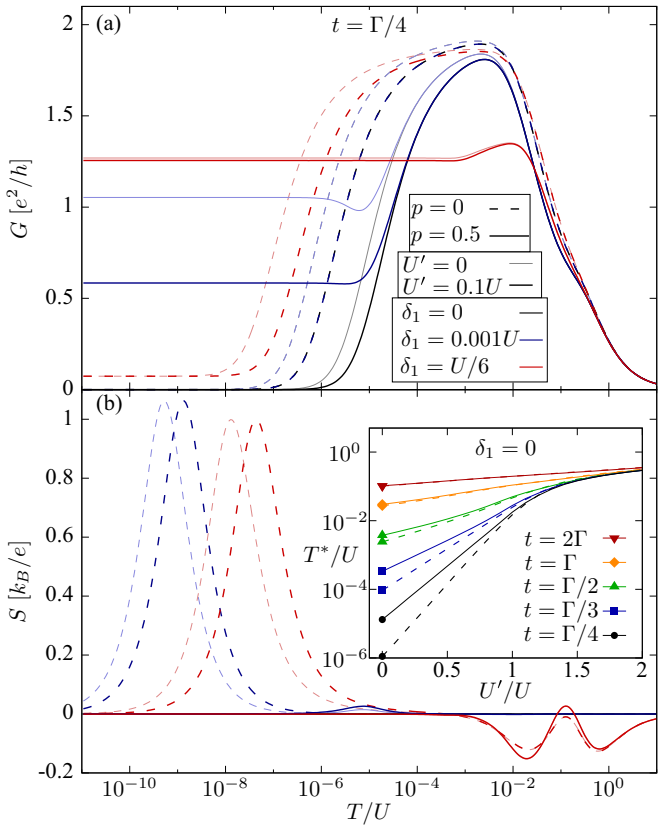

FIG. 2. (a) The conductance G and (b) the Seebeck coefficient S as functions of temperature T for different detunings δ_1, $U_1 = U_2 = U = D/10$, $\Gamma = U/5$, and $t = \Gamma/4$. Here, D is the band halfwidth used as the energy unit. Solid lines correspond to finite spin polarization of the leads, $p = 0.5$, while dashed lines were used for $p = 0$. Thick (bright thin) lines indicate the presence (absence) of interdot Coulomb interaction $U' = U/10$. The inset shows the dependence of the second-stage Kondo temperature T^* on U' for the particle-hole symmetric case and different t.

PHS point. There, the role of the leads' spin polarization p is reduced to a change in T_K [77] and, thus, the following change in T^*; cf. Eq. (4).

A small detuning from the PHS point results in only quantitative changes for $p = 0$, yet it completely changes the situation for finite p. As clearly visible in Fig. 2(a), $G(T)$ does not drop to 0 at low temperatures for finite δ_1. However, the residual conductance is quite small even for relatively large detunings in the case of $p = 0$, while for finite p, the conductance remains large at low T. This is caused by the exchange field induced by the ferromagnetic leads [9,78]. This exchange field strongly depends on the position of the quantum-dot levels and vanishes precisely at the PHS point [9,78]. Once the exchange field becomes larger than T^* (which is in fact very small), the second stage of the Kondo effect is blocked and the conventional (i.e., single-stage) Kondo effect is restored. On the other hand, for large detunings [compare the curve for $\delta_1 = U/6$ in Fig. 2(a)], the exchange field is comparable to T_K and also the conventional Kondo effect becomes blocked.

In the inset of Fig. 2, the dependence of T^* on U' is presented for a few values of t and $p = 0$ (dashed lines) as well as $p = 0.5$ (solid lines). It was extracted from $G(T)$ dependences calculated for different U'. As reported earlier by Ferreira and co-workers for the case of nonmagnetic leads [7], the capacitative coupling between the dots tends to increase J and leads to exponential increase of T^* in the physically relevant regime of $U' < U$. This remains true also for ferromagnetic leads. Actually, the presence of Coulomb correlations between the dots reduces the difference between the cases of finite p and $p = 0$, which is an interesting result at the PHS point, where the only influence of p is the $T_K(p)$ dependence.

Additional information about the relevant regimes can be extracted from the temperature dependence of the thermopower S [10,40]. However, to achieve finite values of the Seebeck coefficient, one needs to tune the system from the PHS point, where $S = 0$. Let us now inspect this in more detail for the line corresponding to $p = 0$, $\delta_1 = U/6$, and $U' = U/10$ shown in Fig. 2(b). At high temperatures, the system is in the hopping transport regime [44,45], characterized by $S \sim T^{-1}$. The negative sign of S is caused by the fact that positive frequencies host more spectral weight. Then, with decreasing the temperature, S exhibits first a local minimum and then, while cooling the system further, its sign changes twice, before another minimum occurs. The narrow region of positive thermopower corresponds to the Coulomb blockade regime, which is hardly present due to relatively strong coupling $\Gamma = U/5$ used in Fig. 2. The second minimum in S is a consequence of asymmetric Kondo peak near the Fermi level. Despite the fact that T_K depends on p [77], the position of the minimum related to the Kondo effect is practically independent of p. Moreover, it also hardly depends on U'; cf. Fig. 2(b). This is not the case for the position of the maximum in thermopower, which is present at even lower temperatures and is related to the second stage of screening. One can also see that the maximum is completely absent for $p = 0.5$, which is due to the fact that for assumed parameters, the exchange field is larger than T^* and the second stage of screening is suppressed; compare with Fig. 2(a). Furthermore, as far as the effect of U' is concerned, the shift of the maximum in S due to capacitive coupling can be visible and it results from the corresponding change in T^*, which can be seen in the temperature dependence of the conductance.

Finally, it is worthwhile to note that the maximum of S at $T \sim T^*$ is much more pronounced as compared to the minimum at $T \sim T_K$. This is caused by the fact that good thermoelectric materials are characterized by sharp and asymmetric features in the spectral density near $\omega = 0$ [79,80]. For the parameters considered in Fig. 2, the Kondo temperature T_K is quite large and the Kondo peak in the spectral density is relatively broad. On the contrary, T^* is indeed cryogenic, and the dip in $\mathcal{T}(\omega)$ corresponding to the second stage of screening is very sharp.

B. Influence on Fano interference and its spin dependence

The Fano effect is a consequence of the quantum interference between a resonant level and the continuum of states [13]. It is therefore also present in DQD systems (even noninteracting) and manifests itself through an antiresonance in the conductance as a function of DQD energy levels [14]. Finite

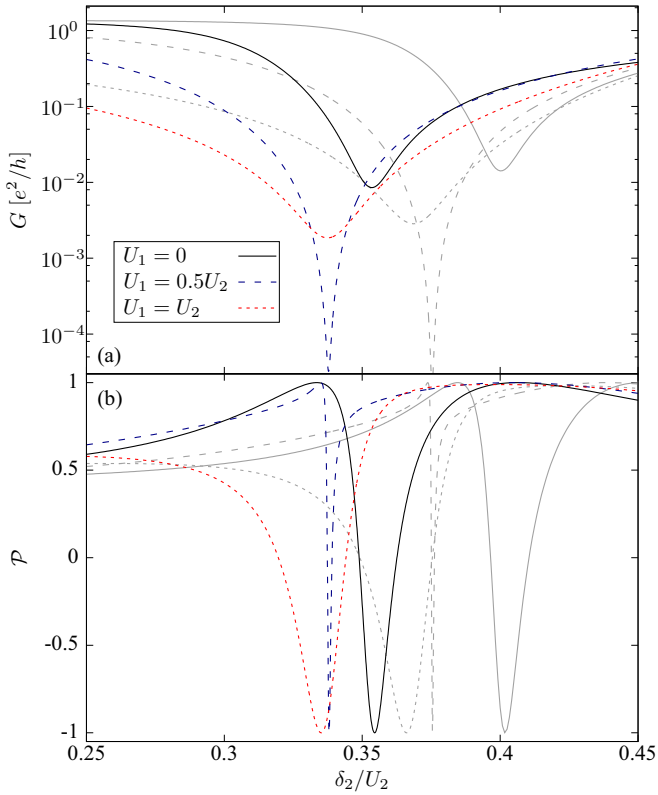

FIG. 3. (a) The low-temperature conductance G and (b) its spin polarization $\mathcal{P}$ plotted as a function of QD2 detuning δ_2 for ferromagnetic leads ($p = 0.5$), $\delta_1 = -0.1U_2$, $U' = 0.1U_2$, $U_2 = D/10$, and different U_1, as indicated. For comparison, the same curves calculated for the case of $U' = 0$ are shown using a light-gray color.

Coulomb correlations can modify the conditions for Fano interference and result in other interesting phenomena. Primarily, the Fano physics is obtained only at the zero-temperature limit, which may be experimentally irrelevant due to the cryogenic scale of T^* occurring in the system. At finite T, deviations from the Fano antiresonance curve can be expected and have already been measured [6,15]. In fact, the antiresonance itself may be seen as the consequence of the second stage of the Kondo effect, which leads to the suppression of the conductance at $T \ll T^*$ [6]. Moreover, when $U_2 > 0$, a spin splitting of the conductance antiresonance occurs in T-shaped DQD coupled to ferromagnetic leads without applying an external magnetic field [17].

The Fano-like antiresonance is visible in Fig. 3(a), where the conductance is plotted against detuning of the QD2 energy level for a few values of the Coulomb interaction strengths of QD1, U_1. Clearly, for all considered values of U_1, the minimum in $G(\delta_2)$ is present (note the logarithmic scale on the vertical axis). The total conductance does not drop to 0 due to the spin splitting of the resonance condition, which can be recognized from the plot of conductance spin polarization $\mathcal{P}$ in Fig. 3(b). The latter varies continuously between $\mathcal{P} = -1$ (for δ_2 corresponding to the antiresonance in the majority spin channel) and $\mathcal{P} = 1$ (for antiresonance in the minority channel). Qualitatively, this situation is hardly changed by finite Coulomb interactions in QD1 U_1 or the interdot capacitative coupling U'. It can be seen that U_1 slightly changes the position of the antiresonance and affects its width and depth. On the other hand, U' only shifts the minima, not affecting their depth or spin splitting significantly, as can be seen from comparison with the $U' = 0$ case, which is plotted in Fig. 3 with bright lines.

Based on these observations, one could naively think that a weak coupling of SC lead to QD1, effectively resulting in a reduction of U_1 to $\tilde{U}_1 = \sqrt{U_1^2 - 4\Gamma_{S1}^2}$, should only quantitatively influence the Fano effect and its spin dependence. As shall be shown in Sec. IV C, this conjecture is not true.

Summing up this section, we have found that the presence of capacitive correlations between the two quantum dots does not change the qualitative features of the presented results. However, the quantitative changes can be relatively strong due to the exponential dependence of T^* on U'. Therefore, to make the analysis more realistic, from now on we assume $U' = U/10$, which is a reasonable value for typical experimental setups [81], and discuss its influence on the results whenever important.

IV. EFFECT OF PAIRING INDUCED IN THE FIRST QUANTUM DOT

In this section, we describe the properties of T-shaped DQD, in which the first quantum dot is proximized by the superconductor; see Fig. 1(a). In Sec. IV A, we analyze how the superconductor proximity affects the two-stage Kondo effect in the considered system. Then, in Sec. IV B, we examine the influence of the interdot hopping on the phase transition in QD1 [34]. The interplay between the spin-dependent Fano interference and the pairing induced by the SC lead is discussed in Sec. IV C.

A. Influence of pairing correlations on the two-stage Kondo effect

The influence of the superconductor proximity on the two-stage Kondo effect can be understood by resorting to the single-quantum-dot case, for which it was shown that finite Γ_{S1} ($\Gamma_{S2} = 0$) results in an enhancement of the Kondo temperature [33,34]. One can thus expect, through exponential dependence of T^* on T_K [cf. Eq. (4)], that even a small increase in T_K should give rise to much larger changes in T^*. This can be clearly seen in Fig. 4(a), which presents the conductance plotted against T for a few representative values of Γ_{S1}. Indeed, while increasing the strength of coupling to the superconductor results in a slight enhancement of T_K, the second-stage Kondo temperature exhibits a strong suppression with raising Γ_{S1}. Additionally, for $\Gamma_{S1} < U/4$, one finds $G(T = 0) \approx \alpha\Gamma_{S1}^2/U^2$, with $\alpha \approx 3$. Moreover, the local maximum in $G(T)$ is slightly lowered as Γ_{S1} increases. This can be understood by referring to the case of a proximized quantum dot, where the low-temperature value of the conductance was found to be suppressed due to the coupling to the superconductor [33,34]. We also note that both the low-temperature conductance as well as the local maximum in $G(T)$ are rather independent of U', although for $U' = 0$ the minimum is achieved at slightly lower T, due to smaller T^*; see Fig. 4(a).

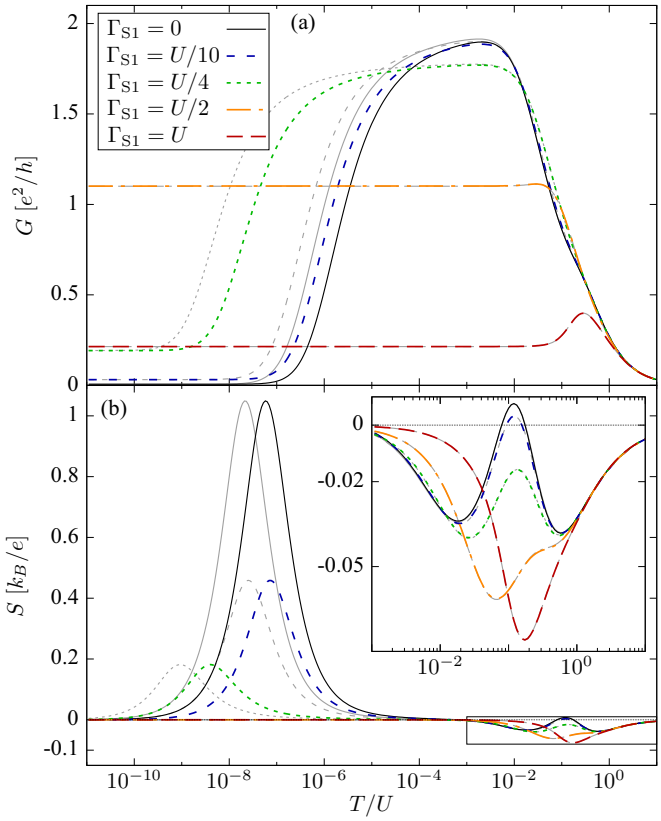

FIG. 4. (a) The conductance G and (b) thermopower S as a function of temperature T calculated for $U_i = U = D/10$, $U' = U/10$, and different values of coupling to superconducting lead Γ_{S1} at $\delta_1 = 0.05U$ and $p = 0$. The case of $U' = 0$ is shown with bright lines for comparison. The inset shows a close-up on the region of high T in (b), marked by the rectangle in the main figure.

Figure 4(b) presents how the finite value of coupling Γ_{S1} affects the thermopower of the system. The most visible feature is that unlike the conductance, the Seebeck coefficient is very sensitive to the presence of SC correlations. Already, as small a pairing potential as the one induced by $\Gamma_{S1} = U/10$ leads to the reduction of the maximal value of S to less than a half of the value for $\Gamma_{S1} = 0$. One could claim that at low temperatures, the thermopower is proportional to T and this reduction can be understood as a consequence of the decrease of T^*. However, usually the lower T^* corresponds to the sharper dip in the spectral density, which compensates for the decrease of T^*. In fact, when reducing the second-stage Kondo temperature T^* by decreasing the hopping between the dots t, the maximum in S remains almost constant for $t < \Gamma/2$ [10]. Moreover, according to Fig. 4, the decrease caused by neglecting U' also does not lead to the suppression of S, despite the fact that the corresponding decrease of T^* is practically identical to the one caused by $\Gamma_{S1} = U/10$; cf. Fig. 4(a). One can conclude that the suppression of the thermopower by the SC proximity effect cannot be explained by the effective reduction of the Coulomb interactions and can be seen as a manifestation of the sensitivity of caloric properties against the pairing correlations.

The values of thermopower at higher temperatures are much smaller than at $T \sim T^*$, as already explained in Sec. III A. However, the zoom of S in this regime (see the inset in Fig. 4) unveils further interesting properties. First of all, as can be intuitively understood through the effective reduction of U_1, the positive peak of $S(T)$ corresponding to the Coulomb blockade regime is quickly suppressed with increasing Γ_{S1}. Furthermore, the negative peak related to the Kondo regime is enhanced and, for strong Γ_{S1}, ultimately merges with the negative peak corresponding to the thermal accessibility of the Hubbard peaks; see the curve for $\Gamma_{S1} = U$. This behavior, clearly different from that for the second stage of screening, shows that the competition between the SC correlations and good thermoelectric properties is not a general rule.

B. Influence of interdot hopping on the phase transition

For negligible interdot hopping $t = 0$, the system considered here is reduced to the case of a single quantum dot proximized by the SC lead, which has been studied, e.g., in Ref. [34], in the context of the phase transition between the Kondo singlet and the singlet being a superposition of empty and doubly occupied states of the dot, where the expectation value $\langle d_{1\uparrow} d_{1\downarrow} \rangle$ becomes nonzero. This transition is a sharp quantum phase transition in the limit $\Gamma \to 0$ only, while in the presence of normal leads it becomes a smooth crossover of the width $\sim\Gamma$. In the following section, we analyze the effect of finite hopping t between the two dots on this crossover. To achieve this, we analyze the dependence of conductance, Seebeck coefficient, and the *order parameters* $\langle d_{1\uparrow} d_{1\downarrow} \rangle$ and $\langle d_{2\uparrow} d_{2\downarrow} \rangle$ as functions of the coupling to the SC lead, which are shown in Fig. 5. The coupling of QD1 to the normal leads Γ was reduced in comparison to Fig. 4 to prevent the crossover from becoming very wide. In this way, we can make reference to the physics of the quantum phase transition, which only gets smeared due to finite Γ. We also use the cryogenic yet finite temperature $T = 10^{-9}U$, instead of $T = 0$, because for small values of t the second-stage Kondo temperature T^* can be even smaller, which is experimentally completely irrelevant.

For $t = 0$, the conductance smoothly changes from almost $G = 2e^2/h$ at $\Gamma_{S1} = 0$ due to the conventional Kondo effect (the value is slightly lower due to small detuning from PHS) to $G \approx 0$ for strong Γ_{S1}, where the Kondo resonance at the Fermi energy is destroyed by the pairing correlations. As far as the thermopower is concerned, one could expect a negative peak at $T \sim T_K$. However, at low temperatures, $S \sim T$ [40], as follows from the Sommerfeld expansion, and for the considered very low temperature, one gets $S \approx 0$. The crossover of the order parameter at QD1 in the case of $t = 0$ from $\langle d_{1\uparrow} d_{1\downarrow} \rangle = 0$, in the absence of the SC lead, to the universal limit $\langle d_{1\uparrow} d_{1\downarrow} \rangle = 1/2$, for $\Gamma_{S1} \to \infty$, can be seen in Fig. 5(c). Obviously, at the decoupled QD2, $\langle d_{2\uparrow} d_{2\downarrow} \rangle = 0$. We note that the above discussed results are also valid for finite t, as long as the hopping is small enough, so that $T^* \ll T$. Otherwise, the landscape changes significantly.

For $\Gamma = U/20$, as assumed in Fig. 5, a finite value of hopping of the order of $t = \Gamma/25 = U/500$ is already large enough to result in almost full development of the second stage of screening for $\Gamma_{S1} = 0$ at the considered temperature. However, finite Γ_{S1} increases T_K and, consequently, decreases T^* [compare Eq. (4) and Fig. 4], leading to the restoration of the conventional Kondo effect (suppression of its second stage of screening) for some critical Γ_{S1}; see the curves for

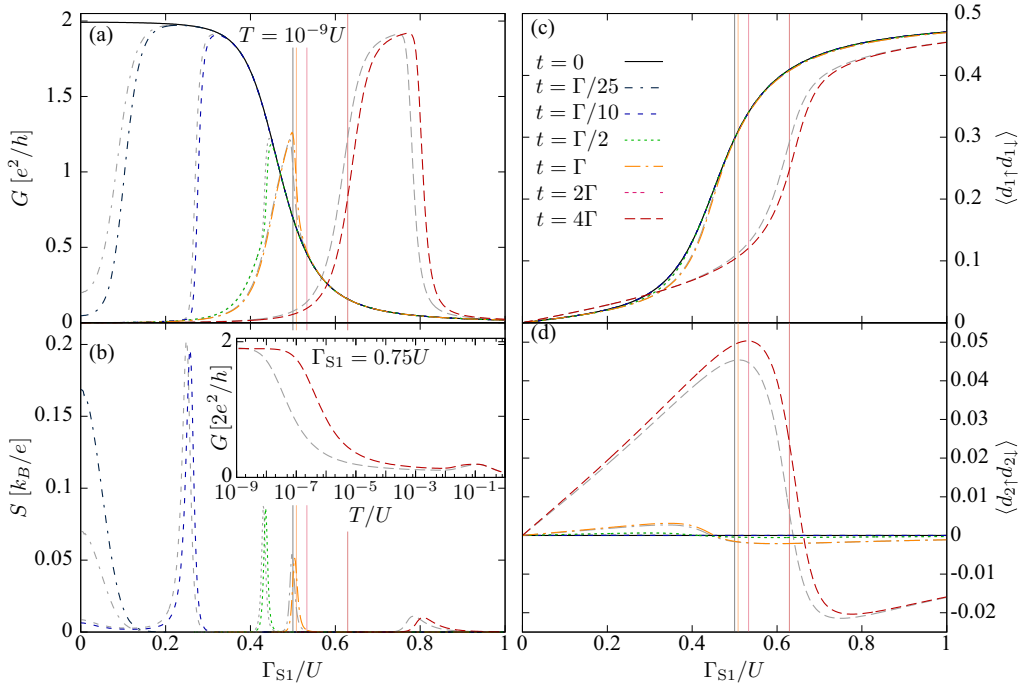

FIG. 5. (a) The conductance G, (b) the Seebeck coefficient S, and the expectation values (c) $\langle d_{1\uparrow}d_{1\downarrow}\rangle$ and (d) $\langle d_{2\uparrow}d_{2\downarrow}\rangle$ as functions of the coupling strength of the first quantum dot to the SC lead Γ_{S1} for a few values of interdot hopping t, as indicated. The other parameters are $\delta_1 = 0.05U$, for $U_1 = U_2 = U = D/10$, $T = 10^{-9}U$, $\Gamma = U/20$, $p = 0$, and $U' = U/10$. The case of $U' = 0$ is shown for comparison with bright lines. The inset in (b) presents the temperature dependence of the conductance for $\Gamma_{S1} = 0.75U$ and $t = 4\Gamma$. Vertical lines correspond to the singlet-doublet transition point for a device decoupled from normal leads, corresponding to $t = 0$ and $t \geqslant \Gamma$.

$t = \Gamma/25$ and $t = \Gamma/10$ in Fig. 5(a). This critical value of Γ_{S1}^* corresponds to $T^*(\Gamma_{S1} = \Gamma_{S1}^*) = T$. As explained in Sec. IV A, for $T \approx T^*$, one can expect a large, positive peak in $S(T)$. This condition is fulfilled around $\Gamma_{S1} = \Gamma_{S1}^*$ and, therefore, the corresponding peak of $S(\Gamma_{S1})$ can be observed in Fig. 5(b). Again, for $t \leqslant U/40$, the couplings $\Gamma_{S1} \gtrsim U/2$ lead to the crossover to the Shiba state and the suppression of the Kondo effect, with almost unaffected $\langle d_{1\uparrow}d_{1\downarrow}\rangle(\Gamma_{S1})$ dependence and very small values of $\langle d_{2\uparrow}d_{2\downarrow}\rangle$. In this sense, the crossover is qualitatively unaffected by the presence of QD2, provided $t \ll \Gamma$.

Finally, let us analyze what happens for stronger values of hopping $t \gtrsim \Gamma$. Then, for $\Gamma_{S1} = 0$, the local singlet inside the DQD is formed and the Kondo effect is completely suppressed [4]. The transport is governed by the spectrum of H_{SDQD} and the matrix elements of $d_{1\sigma}$ between its eigenstates. When Γ_{S1} is increased, at the critical value of Γ_{S1}, the ground state of H_{SDQD} becomes a spin doublet. In the limit of small t, this doublet corresponds to a single electron in QD2 and QD1 in the superconducting singlet state. Therefore, the doublet is practically decoupled from the leads and the Kondo effect is suppressed. However, interdot hybridization restores the matrix element of $d_{1\sigma}$ between the aforementioned doublet and the excited states. Then, the Kondo effect is always present, although the corresponding Kondo temperature $\tilde{T}_K$ vary strongly with Γ_{S1}. In particular, when the singlet-doublet splitting becomes very large, the relevant Kondo scale is strongly suppressed. This is visible in Fig. 5(a) for $t = U/5$. On the other hand, for $\Gamma_{S1} \sim 0.75U$, the Kondo effect is restored, as seen also in the inset, where the temperature dependence of conductance for such a case is plotted. Higher values of Γ_{S1} correspond to larger singlet-doublet splitting, hence the drop of T_K below the temperature assumed for calculations in the figure. We note that a similar suppression of the Kondo effect due to singlet-doublet splitting was also reported in the case of DQDs in a Cooper pair splitting geometry [82].

It seems worth emphasizing that the restoration of the Kondo effect for large t does not have the nature of suppressing the second stage of the Kondo effect. On the contrary, it happens rather at QD2, while QD1 only mediates the coupling to the leads. This resembles the situation when QD1 is very far from particle-hole symmetry, described in Ref. [8]. Interestingly, the positive peak of $S(\Gamma_{S1})$ is only diminished but not completely suppressed in this regime. However, it no longer coincides with the maximum of the $G(\Gamma_{S1})$ slope. Moreover, for strong t, the order parameter at QD2 becomes nonzero; see Fig. 5(d). As long as the ground state of H_{SDQD} is a spin singlet, $\langle d_{2\uparrow}d_{2\downarrow}\rangle > 0$, i.e., the order parameter in the second dot has the same sign as $\langle d_{1\uparrow}d_{1\downarrow}\rangle$. However, $\langle d_{2\uparrow}d_{2\downarrow}\rangle(\Gamma_{S1})$ changes sign at critical Γ_{S1}, corresponding approximately to the singlet-doublet transition in a DQD isolated from the normal leads. The critical values for the transition are indicated in Fig. 5 by vertical lines. The sign change of the pairing expectation value may be understood by recalling the fact that this is in fact expected beyond the $\Delta \to \infty$ approximation, i.e., when quasiparticle states in SC are also available [75]. Since QD2 is proximized by the continuum of states formed by QD1 and the leads, exhibiting also pairing correlations, the sign change of its order parameter at the singlet-doublet transition is visible. The difference between the zero of $\langle d_{2\uparrow}d_{2\downarrow}\rangle(\Gamma_{S1})$ and

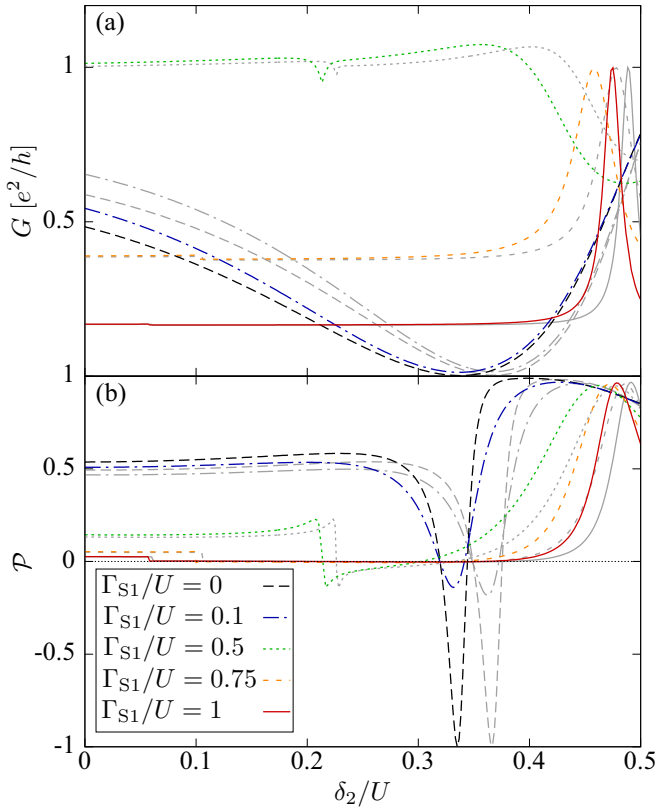

FIG. 6. (a) The low-temperature conductance G and (b) its spin polarization $\mathcal{P}$ as a function of QD2 detuning δ_2 for different couplings Γ_{S1} between the QD1 and SC lead, and $U_1 = U_2 = U = D/10$, $\Gamma = U/5$, $t = \delta_1 = U' = U/10$, and $p = 0.5$. Bright lines indicate the results in the case of $U' = 0$, for comparison.

the value of Γ_{S1} corresponding to the singlet-doublet transition is a consequence of renormalization of DQD levels due to finite coupling to normal leads Γ.

C. Influence of pairing correlations on the spin-dependent Fano effect

From the discussion in previous sections, one can see that in many cases, the main effect of the presence of a weakly coupled superconducting lead is an effective decrease of the relevant Coulomb interaction. However, this is not always the case, as argued in this section. As shown in Sec. III B, in the case of ferromagnetic leads and $U_2 \neq 0$, the spin-dependent Fano effect is present irrespective of the Coulomb interaction strength in the first quantum dot, U_1. Nevertheless, even relatively small values of Γ_{S1} result in a practically complete suppression of the spin splitting of the minimum in conductance. This is visible in Fig. 6, presenting the conductance and its spin polarization as functions of δ_2 for $U_1 = U_2 = U$ and for a few representative values of Γ_{S1}. Although relatively low values of coupling Γ_{S1} do not suppress the minimum in $G(\delta_2)$ [see curve for $\Gamma_{S1} = 0.1U$ in Fig. 6(a)], the spin-filtering effect is completely suppressed, as presented in Fig. 6(b). Note that such a suppression effect was not obtained by altering only U_1 in Sec. III B. Moreover, this effect does not depend on U' either, as can be seen by comparison to the case of $U' = 0$ shown with bright lines in Fig. 6. The fragility of the spin dependence of the Fano interference to the superconducting proximity effect is, therefore, a consequence of a nontrivial interplay between the pairing and the spin correlations.

In the case of stronger coupling Γ_{S1}, even more dramatic changes can be expected. Indeed, the Fano antiresonance is completely removed for $\Gamma_{S1} \geqslant 0.5U$; see Fig. 6(a). Moreover, the transition between the singlet and doublet ground states of H_{SDQD} can give rise to the change of sign of the spin polarization, as observed in Fig. 6(b); see, for example, the curve for $\Gamma_{S1} = 0.5U$ at $\delta_2 \approx 0.22U$. Nevertheless, the suppression of conductance is not complete in any of the spin channels and the absolute value $|\mathcal{P}|$ does not exceed 25% in this regime. One can thus conclude that superconducting pairing correlations have a clearly detrimental effect on the spin-filtering properties of the considered device.

V. EFFECT OF PAIRING INDUCED IN THE SECOND QUANTUM DOT

In the preceding section, the focal point of the discussion was the phase transition in QD1 and its influence on the Kondo physics of the system. Now, in turn, we move to the analysis of transport properties of a different setup, which is shown in Fig. 1(b). Even though the physics for small pairing correlations is in such a case quite similar to the case of the system presented in Fig. 1(a), there appear significant differences which are discussed in the following.

In the present section, the analysis of the Kondo effect is continued for the case of small particle-hole asymmetry, allowing for a nonzero Seebeck coefficient to occur. The normal leads are assumed to be nonmagnetic. The Fano-like interference effects occur to be very similar as in the case of pairing present in QD1 and are not discussed in detail. In particular, small values of Γ_{S2} lead to the Fano antiresonance with a suppressed spin-filtering effect, while strong pairing correlations induced in the second quantum dot destroy the Fano effect completely.

A. Influence of pairing correlations on the two-stage Kondo effect

For weak coupling between the second quantum dot and the SC lead, $\Gamma_{S2} \ll U$, the qualitative understanding of the proximity effect can be founded on the idea of effective reduction of U_2. Therefore, the Kondo temperature for the first stage of screening the spin in the first quantum dot, T_K, hardly depends on Γ_{S2}. Furthermore, from Eq. (4), one immediately recognizes that T^* depends on U_2 through J, and grows with decreasing U_2. Thus, for the device shown in Fig. 1(b), T^* increases with Γ_{S2} in a way similar to T_K increasing with Γ_{S1} for the one presented in Fig. 1(a). Note that this is opposite to what happens to T^* then. This is illustrated in Fig. 7(a) for a few representative values of Γ_{S2}. The corresponding change in the Seebeck coefficient peak position can be observed in Fig. 7(b).

The physics changes, in comparison to pairing induced at QD1, for stronger interdot hopping t. Here, the change of the H_{SDQD} ground state corresponds to the formation of a singlet in QD2, which suppresses the second stage of the Kondo effect

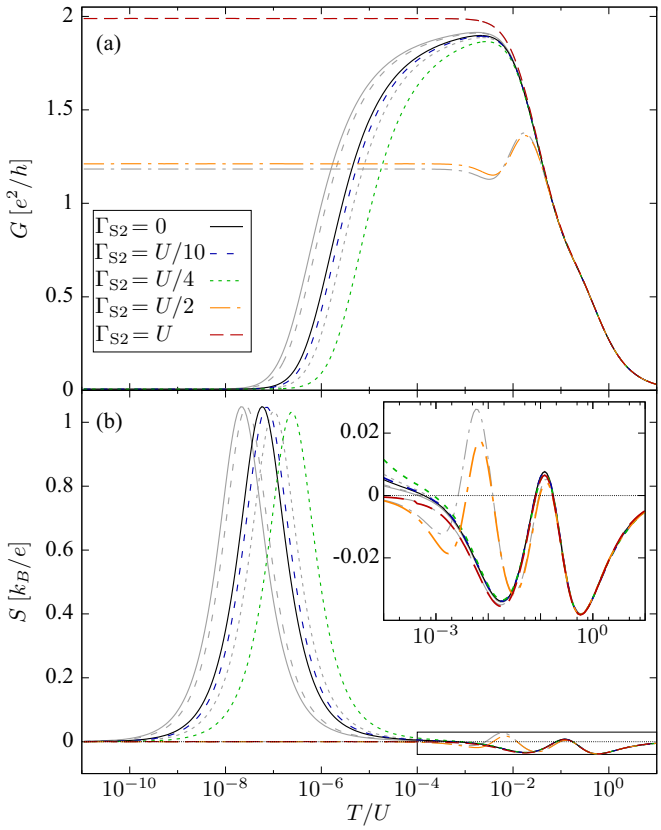

FIG. 7. (a) The conductance G and (b) the Seebeck coefficient S as functions of the temperature T for different couplings Γ_{S2} between the second dot and the SC lead calculated for $\delta_1 = 0.05U$. The other parameters are $U_1 = U_2 = U = D/10$, $\Gamma = U/5$, $t = \Gamma/4$, $p = 0$, and $U' = U/10$. The case of $U' = 0$ is shown with bright lines for comparison. The inset shows the zoom into the large temperature region, marked by a rectangle in the main plot.

for Γ_{S2} above the critical value $\Gamma^*_{S2} \approx U/2$. This is reflected in the perfect conductance and lack of the thermopower peak at low temperatures for $\Gamma_{S2} > \Gamma^*_{S2}$ (for $t > 0$ and $\Gamma > 0$, the transition is in fact a quite sharp crossover, as explained in the following section). Interestingly, an additional sign change of $S(T)$ occurs at $T \sim T_K$ for Γ_{S2} close to this critical value, as illustrated in the inset of Fig. 7(b). This may be accounted for by the splitting of the Kondo peak by a residual dip corresponding to the second stage of screening. In fact, T^* increases with Γ_{S2} quite strongly and becomes only slightly smaller than T_K for $\Gamma_{S2} \approx 0.4U$. Then, the slope of the QD1 spectral function at $\omega = 0$ changes and implies the sign change of S. Nevertheless, for even stronger Γ_{S2}, the second stage of the Kondo effect becomes finally suppressed. Interestingly, the width of the dip in QD1 spectral density corresponding to the second stage of screening (which can be taken as a measure of T^*) is in fact still finite and even growing further, and only its depth vanishes, and so does the related positive peak of $S(T)$ together with the two corresponding sign changes.

B. Phase transition in the second quantum dot

The largest difference between the phase transition at QD1 and the one at QD2 induced by pairing correlations is associated with the fact that while QD1 is directly coupled to the metallic leads, QD2 is coupled only through QD1. Therefore, the effective broadening of QD2 levels is in the leading order proportional to $\Gamma_2 \equiv t^2/\Gamma$. To explore the Kondo correlations, one needs to consider relatively strong coupling Γ, which leads to smearing of the transition at QD1. On the contrary, the transition at QD2 is even sharper for strong Γ. The effect is even more pronounced due to the fact that the interdot hopping t in experimental setups can be quite small. Therefore, the crossover is in fact quite sharp and the similarity to the quantum phase transition, which occurs at $t = 0$ or $\Gamma = 0$, is even more evident than in the case of QD1. However, low values of t also imply indeed cryogenic Kondo temperatures for screening the spin of the second quantum dot, T^*, as follows from Eq. (4). This makes the system vulnerable to perturbations [83] and sets the ground for an interesting interplay between the Kondo effect and the superconducting pairing correlations in the vicinity of the crossover region.

The main results concerning the influence of the interdot coupling on the phase transition at QD2 are summarized in Fig. 8. Similarly to Fig. 5, a finite yet very small $T = 10^{-9}U$ was assumed in calculations. For $t = 0$, there is a strict phase transition, with discontinuous change of the order parameter $\langle d_{2\uparrow} d_{2\downarrow} \rangle$ at $\Gamma_{S2} = U/2$, as shown in Fig. 8(c). At the same time, there are no consequences of this fact for transport properties between the normal leads since QD2 remains completely decoupled from them. Therefore, the conventional, single-stage Kondo effect takes place and the conductance $G = G_{max}$ does not depend on Γ_{S2} ($G_{max} < 2e^2/h$ due to particle-hole asymmetry); cf. Fig. 8(a). Similarly, the Seebeck coefficient $S \sim T \approx 0$, as shown in Fig. 8(b).

For finite hopping t, the second stage of the Kondo effect develops at energy scales corresponding to T^*. Nevertheless, at finite temperature, only for sufficiently strong t does T^* exceed the actual T used in calculations. This can be visible for $t = \Gamma/6$ in Fig. 8(a). Moreover, due to the increase of T^* with Γ_{S2}, the relevant critical value of t, at which $T^* = T$, diminishes. Consequently, the conductance is suppressed and a peak appears in $S(\Gamma_{S2})$ dependence; see Fig. 8(b). However, unlike in the case of pairing induced in QD1 discussed in previous sections, the obtained values of S are larger and the thermoelectric efficiency is enhanced. This is illustrated by the thermoelectric figure of merit reaching almost $ZT = 0.25$, as presented in the inset to Fig. 8(b). This should be compared to $ZT \approx 0.01$ for parameters assumed in Fig. 5 (result not shown in the figure). Further increase of the coupling to the SC lead induces a crossover to the conventional Kondo regime. Its width is set up by the effective coupling of QD2 to the normal leads, Γ_2, as can be deduced from Fig. 8(c). Therefore, for strong Γ_{S2}, the conductance is maximized and the thermopower strongly suppressed.

It is interesting to note that in the geometry considered in this section, QD2 and the normal leads do not form a common continuous medium exhibiting pairing correlations, to which QD1 is coupled. For this reason, the pairing amplitude induced in QD1 by the coupling to QD2 is always of the same sign and is simply caused by the hybridization of single-electron states; cf. inset in Fig. 8(c). Nevertheless, the order parameter $\langle d_{1\uparrow} d_{1\downarrow} \rangle$ exhibits a peak at $\Gamma_{S2} = \Gamma^*_{S2}$.

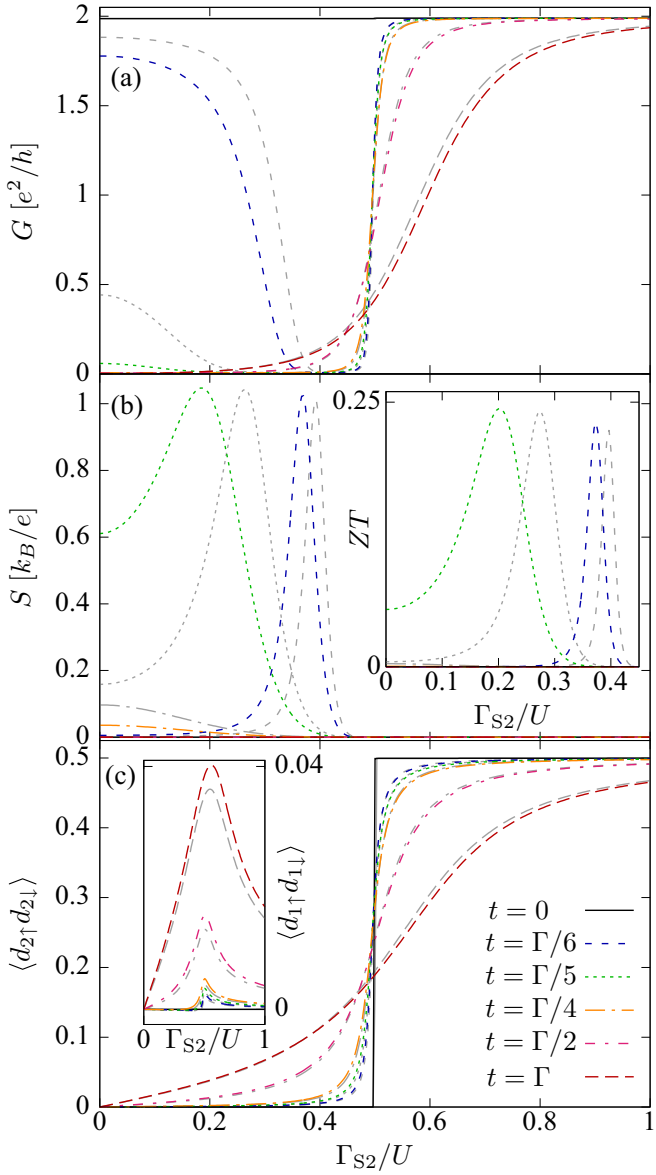

FIG. 8. (a) The conductance G, (b) Seebeck coefficient S, and (c) the order parameter in QD2 $\langle d_{2\uparrow}d_{2\downarrow}\rangle$ as function of coupling between the second quantum dot and the SC lead Γ_{S2} for different interdot hoppings t. The other parameters are $\delta_1 = 0.05U_1$, $U_1 = U_2 = U = D/10$, $\Gamma = U/5$, $p = 0$, $T = 10^{-9}U$, and $U' = 0.1U$. The $U' = 0$ case is shown with bright lines for comparison. The inset in (b) shows the thermoelectric figure of merit ZT as a function of Γ_{S2}. The inset in (c) presents the order parameter in QD1 (note different scale).

Finally, the large-t regime corresponds to the transport through molecular levels of DQD in the proximity of the SC lead. The location of the crossover is only slightly shifted due to the renormalization of the energy levels, but its width is increased significantly due to large Γ_2. As can be seen in the inset in Fig. 8(c), $\langle d_{1\uparrow}d_{1\downarrow}\rangle$ remains positive, which is due to the reasons explained above. Consequently, the strong-t case does not differ quantitatively much from the case corresponding to weaker interdot hopping, unless caloric properties are concerned. Then, of course, smoothed crossover leads to a small slope of the spectral function at $\omega = 0$ and, consequently, reduced thermopower.

VI. CONCLUSIONS

In the present paper, we have analyzed the transport properties of a T-shaped double-quantum-dot system proximized by the superconductor, considering two distinct geometries. In the first one, the quantum dot directly coupled to the normal leads was connected to the superconductor, while in the second geometry, the side coupled quantum dot was proximized. We have thoroughly examined the subgap physics of both devices and showed that depending on the superconductor position, the second-stage Kondo temperature T^* may be either enhanced or decreased by a small coupling to the superconductor. In both cases, there appears a doublet-singlet crossover around some critical value of the SC pairing potential and the properties of the system change completely for strong pairing correlations. Depending on the device's geometry, the conventional Kondo effect may be strongly supported or completely suppressed in this transport regime. Moreover, the crossover becomes very sharp for the superconductor attached to side-coupled quantum dot at the regime of strong coupling to normal leads. We explain these effects as consequence of the effective decrease of the corresponding Coulomb interaction and basic properties of coupled Kondo impurities. Moreover, we show that the spin-dependent Fano-Kondo interference, which develops in the considered systems, turns out to be very vulnerable to the proximity effect. The spin-filtering effects present in T-shaped DQDs with ferromagnetic contacts can be suppressed by even small values of the coupling to the superconductor.

The presented results show that the superconductor proximity effect provides additional means for the control of the two-stage Kondo physics in T-shaped double quantum dots. It enables one to either strongly favor or completely suppress each stage of the Kondo screening and obtain interesting electric or thermoelectric properties. Furthermore, the analysis of transport properties of hybrid T-shaped DQD systems gives additional insight into the nature of the interplay between the Kondo correlations and the superconductivity, which exhibits a surprising combination of increase of the Kondo temperature and suppression of the related spectral features. We hope that our analysis will foster further endeavors in this direction.

ACKNOWLEDGMENTS

This work was supported by the National Science Centre in Poland through Project No. 2015/19/N/ST3/01030. Discussions with B. Bułka are acknowledged.

[1] M. Pustilnik and L. I. Glazman, Kondo Effect in Real Quantum Dots, Phys. Rev. Lett. **87**, 216601 (2001).

[2] M. Vojta, R. Bulla, and W. Hofstetter, Quantum phase transitions in models of coupled magnetic impurities, Phys. Rev. B **65**, 140405(R) (2002).

[3] W. G. van der Wiel, S. De Franceschi, J. M. Elzerman, S. Tarucha, L. P. Kouwenhoven, J. Motohisa, F. Nakajima, and T. Fukui, Two-Stage Kondo Effect in a Quantum Dot at a High Magnetic Field, Phys. Rev. Lett. **88**, 126803 (2002).

[4] P. S. Cornaglia and D. R. Grempel, Strongly correlated regimes in a double quantum dot device, Phys. Rev. B **71**, 075305 (2005).

[5] R. Žitko and J. Bonča, Enhanced conductance through side-coupled double quantum dots, Phys. Rev. B **73**, 035332 (2006).

[6] R. Žitko, Fano-Kondo effect in side-coupled double quantum dots at finite temperatures and the importance of two-stage Kondo screening, Phys. Rev. B **81**, 115316 (2010).

[7] I. L. Ferreira, P. A. Orellana, G. B. Martins, F. M. Souza, and E. Vernek, Capacitively coupled double quantum dot system in the Kondo regime, Phys. Rev. B **84**, 205320 (2011).

[8] Y. Tanaka, N. Kawakami, and A. Oguri, Crossover between two different Kondo couplings in side-coupled double quantum dots, Phys. Rev. B **85**, 155314 (2012).

[9] K. P. Wócik and I. Weymann, Two-stage Kondo effect in T-shaped double quantum dots with ferromagnetic leads, Phys. Rev. B **91**, 134422 (2015).

[10] K. P. Wójcik and I. Weymann, Thermopower of strongly correlated T-shaped double quantum dots, Phys. Rev. B **93**, 085428 (2016).

[11] N. J. Craig, J. M. Taylor, E. A. Lester, C. M. Marcus, M. P. Hanson, and A. C. Gossard, Tunable non-local spin control in a coupled quantum dot system, Science **304**, 565 (2004).

[12] G. Granger, M. A. Kastner, I. Radu, M. P. Hanson, and A. C. Gossard, Two-stage Kondo effect in a four-electron artificial atom, Phys. Rev. B **72**, 165309 (2005).

[13] U. Fano, Effects of Configuration Interaction on Intensities and Phase Shifts, Phys. Rev. **124**, 1866 (1961).

[14] T.-S. Kim, S. Hershfield, Suppression of current in transport through parallel double quantum dots, Phys. Rev. B **63**, 245326 (2001).

[15] S. Sasaki, H. Tamura, T. Akazaki, and T. Fujisawa, Fano-Kondo Interplay in a Side-Coupled Double Quantum Dot, Phys. Rev. Lett. **103**, 266806 (2009).

[16] L. G. G. V. Dias da Silva, E. Vernek, K. Ingersent, N. Sandler, and S. E. Ulloa, Spin-polarized conductance in double quantum dots: Interplay of Kondo, Zeeman and interference effects, Phys. Rev. B **87**, 205313 (2013).

[17] K. P. Wójcik and I. Weymann, Perfect spin polarization in T-shaped double quantum dots due to the spin-dependent Fano effect, Phys. Rev. B **90**, 115308 (2014).

[18] Y. Tanaka, N. Kawakami, and A. Oguri, Andreev transport through side-coupled double quantum dots, Phys. Rev. B **78**, 035444 (2008).

[19] J. Barański and T. Domański, Fano-type interference in quantum dots coupled between metallic and superconducting leads, Phys. Rev. B **84**, 195424 (2011).

[20] J. Barański and T. Domański, Decoherence effect on Fano line shapes in double quantum dots coupled between normal and superconducting leads, Phys. Rev. B **85**, 205451 (2012).

[21] A. M. Calle, M. Pacheco, and P. A. Orellana, Fano effect and Andreev bound states in T-shape double quantum dots, Phys. Lett. A **377**, 1474 (2013).

[22] J. Barański and T. Domański, Fano-type resonances induced by a boson mode in Andreev conductance, Chin. Phys. B **24**, 017304 (2015).

[23] A. M. Calle, M. Pacheco, G. B. Martins, V. M. Apel, G. A. Lara, and P. A. Orellana, Fano-Andreev effect in a T-shape double quantum dot in the Kondo regime, J. Phys.: Condens. Matter **29**, 135301 (2017).

[24] A. F. Andreev, The thermal conductivity of the intermediate state in superconductors, Zh. Eksp. Teor. Fiz. **46**, 1823 (1964) [J. Exp. Theor. Phys. **19**, 1228 (1964)].

[25] S. De Franceschi, L. Kouwenhoven, C. Schönenberger, and W. Wernsdorfer, Hybrid superconductor-quantum dot devices, Nat. Nano. **5**, 703 (2010).

[26] A. Martin-Rodero and A. Levy Yeyati, Josephson and Andreev transport through quantum dots, Adv. Phys. **60**, 899 (2011).

[27] J. Kondo, Resistance minimum in dilute magnetic alloys, Prog. Theor. Phys. **32**, 37 (1964).

[28] A. C. Hewson, *The Kondo Problem to Heavy Fermions* (Cambridge University Press, Cambridge, 1993).

[29] A. V. Rozhkov and D. P. Arovas, Interacting-impurity Josephson junction: Variational wave functions and slave-boson mean-field theory, Phys. Rev. B **62**, 6687 (2000).

[30] M. R. Buitelaar, W. Belzig, T. Nussbaumer, B. Babić, C. Bruder, and C. Schönenberger, Multiple Andreev Reflections in a Carbon Nanotube Quantum Dot, Phys. Rev. Lett. **91**, 057005 (2003).

[31] K. J. Franke, G. Schulze, and J. I. Pascual, Competition of superconducting phenomena and Kondo screening at the nanoscale, Science **332**, 940 (2011).

[32] J.-D. Pillet, P. Joyez, R. Žitko, and M. F. Goffman, Tunneling spectroscopy of a single quantum dot coupled to a superconductor: From Kondo ridge to Andreev bound states, Phys. Rev. B **88**, 045101 (2013).

[33] K. P. Wójcik and I. Weymann, Proximity effect on spin-dependent conductance and thermopower of correlated quantum dots, Phys. Rev. B **89**, 165303 (2014).

[34] T. Domański, I. Weymann, M. Barańska, and G. Górski, Constructive influence of the induced electron pairing on the Kondo state, Sci. Rep. **6**, 23336 (2016).

[35] L. Yu, Bound state in superconductors with paramagnetic impurities, Acta Phys. Sin. **21**, 75 (1965).

[36] H. Shiba, Classical spins in superconductors, Prog. Theor. Phys. **40**, 435 (1968).

[37] A. I. Rusinov, On the theory of gapless superconductivity in alloys containing paramagnetic impurities, Zh. Eksp. Teor. Fiz. **56**, 2047 (1969) [J. Exp. Theor. Phys. **29**, 1101 (1969)].

[38] E. J. H. Lee, X. Jiang, M. Houzet, R. Aguado, C. M. Lieber, and S. De Franceschi, Spin-resolved Andreev levels and parity crossings in hybrid superconductor-semiconductor nanostructures, Nat. Nanotech. **9**, 79 (2014).

[39] M. Krawiec and K. I. Wysokiński, Thermoelectric effects in strongly interacting quantum dot coupled to ferromagnetic leads, Phys. Rev. B **73**, 075307 (2006).

[40] T. A. Costi and V. Zlatić, Thermoelectric transport through strongly correlated quantum dots, Phys. Rev. B **81**, 235127 (2010).

[41] T. Rejec, R. Žitko, J. Mravlje, and A. Ramšak, Spin thermopower in interacting quantum dots, Phys. Rev. B **85**, 085117 (2012).

[42] R. Žitko, J. Mravlje, A. Ramšak, and T. Rejec, Spin thermopower in the overscreened Kondo model, New J. Phys. **15**, 105023 (2013).

[43] S. Donsa, S. Andergassen, and K. Held, Double quantum dot as a minimal thermoelectric generator, Phys. Rev. B **89**, 125103 (2014).

[44] S. B. Tooski, A. Ramšak, B. R. Bułka, and R. Žitko, Effect of assisted hopping on thermopower in an interacting quantum dot, New J. Phys. **16**, 055001 (2014).

[45] N. F. Mott and E. A. Davis, *Electronic Processes in Non-Crystalline Materials*, 2nd ed. (Oxford University Press, Oxford, 1979).

[46] L. Hofstetter, S. Csonka, J. Nygård, and C. Schönenberger, Cooper pair splitter realized in a two-quantum-dot y-junction, Nature (London) **461**, 960 (2009).

[47] L. G. Herrmann, F. Portier, P. Roche, A. L. Yeyati, T. Kontos, and C. Strunk, Carbon Nanotubes as Cooper-Pair Beam Splitters, Phys. Rev. Lett. **104**, 026801 (2010).

[48] L. Hofstetter, S. Csonka, A. Baumgartner, G. Fülöp, S. d'Hollosy, J. Nygård, and C. Schönenberger, Finite-Bias Cooper Pair Splitting, Phys. Rev. Lett. **107**, 136801 (2011).

[49] J. Schindele, A. Baumgartner, and C. Schönenberger, Near-Unity Cooper Pair Splitting Efficiency, Phys. Rev. Lett. **109**, 157002 (2012).

[50] A. Das, Y. Ronen, M. Heiblum, D. Mahalu, A. V. Kretinin, and H. Shtrikman, High-efficiency Cooper pair splitting demonstrated by two-particle conductance resonance and positive noise cross-correlation, Nat. Commun. **3**, 1165 (2012).

[51] G. Fülöp, S. d'Hollosy, A. Baumgartner, P. Makk, V. A. Guzenko, M. H. Madsen, J. Nygård, C. Schönenberger, and S. Csonka, Local electrical tuning of the nonlocal signals in a Cooper pair splitter, Phys. Rev. B **90**, 235412 (2014).

[52] G. Fülöp, F. Domínguez, S. d'Hollosy, A. Baumgartner, P. Makk, M. H. Madsen, V. A. Guzenko, J. Nygård, C. Schönenberger, A. Levy Yeyati, and S. Csonka, Magnetic Field Tuning and Quantum Interference in a Cooper Pair Splitter, Phys. Rev. Lett. **115**, 227003 (2015).

[53] Z. B. Tan, D. Cox, T. Nieminen, P. Lähteenmäki, D. Golubev, G. B. Lesovik, and P. J. Hakonen, Cooper Pair Splitting by Means of Graphene Quantum Dots, Phys. Rev. Lett. **114**, 096602 (2015).

[54] K. Grove-Rasmussen, G. Steffensen, A. Jellinggaard, M. H. Madsen, R. Žitko, J. Paaske, and J. Nygård, Yu-Shiba-Rusinov screening of spins in double quantum dots, Nat. Commun. **9**, 2376 (2018).

[55] P. W. Anderson, Model for the Electronic Structure of Amorphous Semiconductors, Phys. Rev. Lett. **34**, 953 (1975).

[56] A. Taraphder and P. Coleman, Heavy-Fermion Behavior in a Negative-U Anderson Model, Phys. Rev. Lett. **66**, 2814 (1991).

[57] S. Andergassen, T. A. Costi, and V. Zlatić, Mechanism for large thermoelectric power in molecular quantum dots described by the negative-U Anderson model, Phys. Rev. B **84**, 241107(R) (2011).

[58] I. Weymann, Boosting spin-caloritronic effects by attractive correlations in molecular junctions, Sci. Rep. **6**, 19236 (2016).

[59] M. Dzero and J. Schmalian, Superconductivity in Charge Kondo Systems, Phys. Rev. Lett. **94**, 157003 (2005)

[60] Y. Matsushita, H. Bluhm, T. H. Geballe, and I. R. Fisher, Evidence for Charge Kondo Effect in Superconducting Tl-Doped PbTe, Phys. Rev. Lett. **94**, 157002 (2005).

[61] M. Matusiak, E. M. Tunnicliffe, J. R. Cooper, Y. Matsushita, and I. R. Fisher, Evidence for a charge Kondo effect in $Pb_{1-x}Tl_xTe$ from measurements of thermoelectric power, Phys. Rev. B **80**, 220403(R) (2009).

[62] A. S. Erickson, N. P. Breznay, E. A. Nowadnick, T. H. Geballe, and I. R. Fisher, Correlation of anomalous normal state properties with superconductivity in $Pb_{1-x-y}Tl_xIn_yTe$, Phys. Rev. B **81**, 134521 (2010).

[63] T. A. Costi and V. Zlatić, Charge Kondo Anomalies in PbTe Doped with Tl Impurities, Phys. Rev. Lett. **108**, 036402 (2012).

[64] G. Cheng, M. Tomczyk, S. Lu, J. P. Veazey, M. Huang, P. Irvin, S. Ryu, H. Lee, C. B. Eom, C. S. Hellberg, and J. Levy, Electron pairing without superconductivity, Nature (London) **521**, 196 (2015).

[65] G. Cheng, M. Tomczyk, A. B. Tacla, H. Lee, S. Lu, J. P. Veazey, M. Huang, P. Irvin, S. Ryu, C. B. Eom, A. Daley, D. Pekker, and J. Levy, Tunable Electron-Electron Interactions in $LaAlO_3/SrTiO_3$ Nanostructures, Phys. Rev. X **6**, 041042 (2016).

[66] T.-F. Fang, A.-M. Guo, H.-T. Lu, H.-G. Luo, and Q.-F. Sun, Charge Kondo effect in negative-U quantum dots with superconducting electrodes, Phys. Rev. B **96**, 085131 (2017).

[67] T.-F. Fang, A.-M. Guo, and Q.-F. Sun, Nonequilibrium Kondo effect by the equilibrium numerical renormalization group method: The hybrid Anderson model subject to a finite spin bias, Phys. Rev. B **97**, 235115 (2018).

[68] L. I. Glazman and M. E. Raikh, Resonant Kondo transparency of a barrier with quasilocal impurity states, J. Exp. Theor. Phys. Lett. **47**, 452 (1988) [Pis'ma Zh. Exp. Teor. Fiz. **47**, 378 (1988)].

[69] K. G. Wilson, The renormalization group: Critical phenomena and the Kondo problem, Rev. Mod. Phys. **47**, 773 (1975).

[70] We use the open-access Budapest `fnrg` code; see O. Legeza, C. P. Moca, A. I. Tóth, I. Weymann, and G. Zaránd, arXiv:0809.3143; The code is available at http://www.phy.bme.hu/∼dmnrg/ (unpublished).

[71] F. B. Anders and A. Schiller, Real-Time Dynamics in Quantum-Impurity Systems: A Time-Dependent Numerical Renormalization-Group Approach, Phys. Rev. Lett. **95**, 196801 (2005).

[72] F. B. Anders and A. Schiller, Spin precession and real-time dynamics in the Kondo model: Time-dependent numerical renormalization-group study, Phys. Rev. B **74**, 245113 (2006).

[73] A. Weichselbaum and J. von Delft, Sum-Rule Conserving Spectral Functions from the Numerical Renormalization Group, Phys. Rev. Lett. **99**, 076402 (2007).

[74] I. Weymann and J. Barnaś, Spin thermoelectric effects in Kondo quantum dots coupled to ferromagnetic leads, Phys. Rev. B **88**, 085313 (2013).

[75] A. Oguri, Y. Tanaka, and A. C. Hewson, Quantum phase transition in a minimal model for the Kondo effect in a Josephson junction, J. Phys. Soc. Jpn. **73**, 2494 (2004).

[76] F. D. M. Haldane, Scaling Theory of the Asymmetric Anderson Model, Phys. Rev. Lett. **40**, 416 (1978).

[77] J. Martinek, Y. Utsumi, H. Imamura, J. Barnaś, S. Maekawa, J. König, and G. Schön, Kondo Effect in Quantum Dots Coupled to Ferromagnetic Leads, Phys. Rev. Lett. **91**, 127203 (2003).

[78] J. Martinek, M. Sindel, L. Borda, J. Barnaś, R. Bulla, J. König, G. Schön, S. Maekawa, and J. von Delft, Gate-controlled spin splitting in quantum dots with ferromagnetic leads in the Kondo regime, Phys. Rev. B **72**, 121302(R) (2005).

[79] L. D. Hicks and M. S. Dresselhaus, Effect of quantum-well structures on the thermoelectric figure of merit, Phys. Rev. B **47**, 12727 (1993); Thermoelectric figure of merit of a one-dimensional conductor, **47**, 16631 (1993).

[80] G. D. Mahan and J. O. Sofo, The best thermoelectric, Proc. Natl. Acad. Sci. USA **93**, 7436 (1996).

[81] A. J. Keller, S. Amasha, I. Weymann, C. P. Moca, I. G. Rau, J. A. Katine, H. Shtrikman, G. Zaránd, and D. Goldhaber-Gordon, Emergent SU(4) Kondo physics in a spin-charge-entangled double quantum dot, Nat. Phys. **10**, 145 (2014).

[82] K. Wrześniewski and I. Weymann, Kondo physics in double quantum dot based Cooper pair splitters, Phys. Rev. B **96**, 195409 (2017).

[83] K. P. Wójcik and I. Weymann, Strong spin Seebeck effect in Kondo T-shaped double quantum dots, J. Phys.: Condens. Matter **29**, 055303 (2017).